J Therm Anal Calorim (2012) 110:973–978
DOI 10.1007/s10973-011-1927-5

Phase transition and thermodynamic properties of TiN under pressure via first-principles calculations

Ke Liu · Xiao-Lin Zhou · Hai-Hua Chen · Lai-Yu Lu

Received: 13 July 2011 / Accepted: 16 September 2011 / Published online: 4 October 2011

Abstract The phase transition of TiN from the NaCl structure to the CsCl structure is investigated by the first-principles plane wave pseudopotential density functional theory method, and the thermodynamic properties of the NaCl structures are obtained through the quasi-harmonic Debye model. It is found that the pressures for transition from the NaCl structure to the CsCl structure are 364.1 GPa (for GGA) and 322.2 (for LDA) from equal enthalpies. The calculated ground state properties such as equilibrium lattice constant, bulk modulus, and its pressure derivative are in good agreement with experimental and theoretical data of others. Moreover, the dependences of the relative volume V/V_0 on the pressure P, the Debye temperature Θ_D, and heat capacity C_V on the pressure P and temperature T, as well as the variation of the thermal expansion α with temperature and pressure are also successfully obtained.

Keywords Phase transition · Thermodynamic property · TiN

Introduction

The transition metal compounds (TMC), which crystallize in an NaCl (B1)-structure at ambient pressure, have been a topic of great interest because of their optical, magnetic, and electrical properties. The high-pressure studies on various materials are significantly important both from basic and applied point of view. The transition metal compounds play an important role in solid-state technology, as they have many scientific, industrial, and technological applications [1, 2]. Titanium nitride is a metallic compound characterized by high melting point, ultra-hardness (comparable to that of diamond), good electrical and thermal conductivity, and high resistance to corrosion [3]. The interesting properties of TiN have been studied with many methods in recent years [4, 5]. TiN is presently one of the most important materials for hardness and corrosion resistant coating [6, 7]. Presently interest is also developing within the microelectronic industry for the use of TiN as an electrically conducting barrier [1].

There are large number of experiments devoted to various aspects of TiN film growth [8–10] and many theoretical calculations about elastic modulus for TiN [1, 11, 12]. Although several research groups have experimental and theoretically investigated the pressure induced phase transitions in TiN using different methods. For example, Zhao et al. [13] investigated the behavior of TiN using axial X-ray diffraction under high pressure to 30.1 GPa. Their experimental results suggested an isostructural phase transition at about 7 GPa as shown by the discontinuity of V/V_0 data with pressure. Ahuja et al. [1], with the LDA approximation, studied the structural phase transition of TiN from NaCl structure to CsCl structure as 370 GPa. Chauhan et al. [14]., by using the three body potential model (TBPM) approach, predicted that the phase transition pressure occurs at 310 GPa and found that the magnitude of relative volume change at the transition pressure lies at 9%. So far, there has been considerable controversy for the phase transition of TiN. On the other hand, to the

K. Liu (✉) · X.-L. Zhou · L.-Y. Lu
Department of Physics, Sichuan Normal University, Chengdu 610066, People's Republic of China
e-mail: lkworld@126.com

X.-L. Zhou
e-mail: Zhouxl_wuli@163.com

K. Liu · H.-H. Chen
Institute of Atomic and Molecular Physics, Sichuan University, Chengdu 610065, People's Republic of China

best of our knowledge, the thermodynamic properties of TiN have not previously been reported. So, we here make first-principles calculations on the thermodynamic properties and the phase transition of TiN from NaCl structure to CsCl structure.

Theoretical method

Total energy electronic structure calculations

We here adopt the non-local ultrasoft pseudopotential introduced by Vanderbilt [15], together with the local-density approximation (LDA) [16] and the Perdew–Burke–Ernzerhof (PBE) generalized gradient approximation (GGA) [17] exchange–correlation function. Pseudo atomic calculations are performed for N 2s2 2p3 and Ti 3s2 3p6 3d2 4s2. A kinetic cut-off of plane wave 350 eV and a $10 \times 10 \times 10$ Monkhorst–Pack [18] grid for the Brillouin-zone sampling are used throughout. The threshold of 10^{-7} eV/atom is used to determine whether the self-consistent progress has been converged. All the total energy electronic structure calculations are implemented through the CASTEP code [19, 20].

Thermodynamic properties

By the experimental methods, such as TG, DSC, and NMR, there are many reports on the thermodynamic properties [21–24]. In this study, we also focus on the thermodynamic properties using a different method. We here apply the quasi-harmonic Debye model [25], in which the phononic effects are considered and by which the thermodynamic properties of MgB_2 [26–28], osmium [29], ZnS [30], and GaN [31] are successfully obtained. In the quasi-harmonic Debye model, the non-equilibrium Gibbs function $G^*(V; P, T)$ takes the form of

$$G^*(V;P,T) = E(V) + PV + A_{Vib}[\Theta(V);T] \quad (1)$$

where $\Theta(V)$ is the Debye temperature, and the vibrational term A_{Vib} can be written as [32, 33]

$$A_{Vib}(\Theta;T) = nKT\left[\frac{9}{8}\frac{\Theta}{T} + 3\ln(1-e^{-\Theta/T}) - D(\Theta/T)\right] \quad (2)$$

where $D(\Theta/T)$ represents the Debye integral, n is the number of atoms per formula unit. The non-equilibrium Gibbs function $G^*(V; P, T)$ as a function of $(V; P, T)$ can be minimized with respect to volume V

$$\left(\frac{\partial G^*(V;P,T)}{\partial V}\right)_{P,T} = 0 \quad (3)$$

By solving Eq. 3, one can get the thermal EOS $V(P, T)$. The isothermal bulk modulus B_T, the heat capacity C_{v}, and the thermal expansion coefficient α are given by [34]

$$B_T(P,T) = V\left(\frac{\partial^2 G^*(V;P,T)}{\partial V^2}\right)_{P,T}, \quad (4)$$

$$C_V = 3nk\left[4D(\Theta/T) - \frac{3\Theta/T}{e^{\Theta/T}-1}\right] \quad (5)$$

$$\alpha = \frac{\gamma C_V}{B_T V} \quad (6)$$

Through the quasi-harmonic Debye model, one could calculate the thermodynamics quantities of any temperatures and pressures of TiN from the calculated energy–volume points at $T = 0$ and $P = 0$.

Experimental method

We investigated the compression behavior of TiN using synchrotron radial X-ray diffraction (RXRD) technique under nonhydrostatic compression up to 45.4 GPa in a diamond–anvil cell. We obtained the hydrostatic compression equation of state of TiN. Fitting to the third-order Birch–Murnaghan equation of state, the bulk modulus derived from nonhydrostatic compression data varies from 232 to 353 GPa, depending on angle Ψ, the orientation of the diffraction planes with respect to the loading axis. The RXRD data obtained at $\Psi = 54.7°$ yield a bulk modulus $B_0 = 282 \pm 9$ GPa with pressure derivative B_0' fixed at four, which reported by us earlier [35].

Results and discussion

For both the NaCl and CsCl structures of TiN, we, using both the GGA and the LDA, take a series of lattice constants a to obtain the total energy E and the corresponding primitive cell volume V, and the GGA-calculated results are illustrated in Fig. 1. The calculated equilibrium lattice constants a, zero-pressure bulk modulus B_0, and its pressure derivation B_0' from the Birch–Murnaghan equation of state (EOS) [36] are listed in Table 1, together with experimental data and other theoretical results for the NaCl structure. The agreement among them is good. Unfortunately, there are no other theoretical and experimental data for checking our results for the CsCl structures.

An estimate of the zero-temperature transition pressure between the NaCl and the CsCl structures of TiN may be obtained from the usual condition of equal enthalpies, i.e., the pressure P at which enthalpies, $H = E + PV$, of both phases are the same. Figure 2 shows the enthalpy for GGA

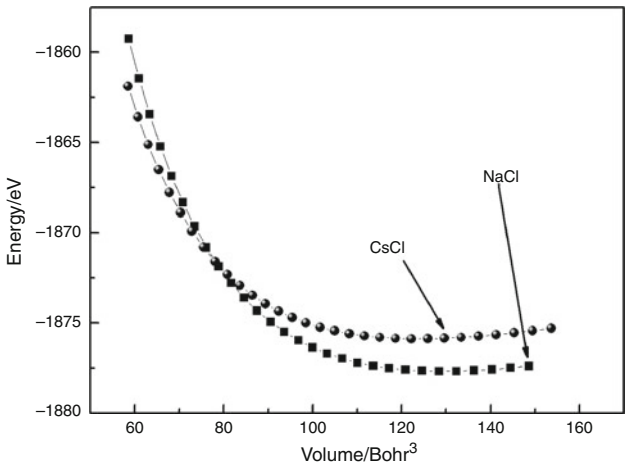

Fig. 1 Total energy (GGA) as a function of primitive cell volume for TiN

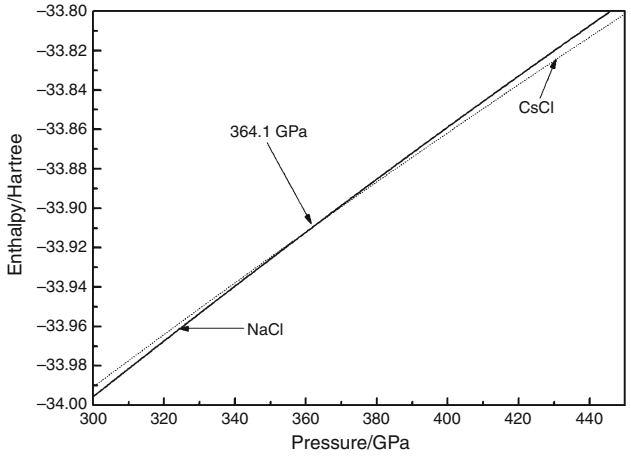

Fig. 2 Enthalpy (GGA) as a function of pressure for TiN

Table 1 The lattice constants, bulk moduli, pressure derivative of bulk modulus of the NaCl structure and CsCl structure of TiN at zero pressure, together with the transition pressures

	Present calc.		Other calc.	Expt.
NaCl structure				
a/Å	4.246 (GGA)	4.175 (LDA)	4.26[a], 4.18[b], 4.175/4.236/4.237/4.260[e], 4.24[h], 4.32[i], 4.253[m]	4.240[j], 4.235[k]
B_0/GPa	277.99	320. 60	286[a], 322[b], 270[c], 310[d] 319/282/282/266[e], 305[h], 389[i], 280[m]	282 ± 9 (present) 320[c], 282[f], 288[i]
$B_0^{'}$	4.30	4.25	4.3/4.2/4.2/4.2[e]	4 (present)
Pt/Gpa	364.1	322.2	370[c], 310[g]	
CsCl structure				
a/Å	2.637	2.585		
B_0/Gpa	253.83	298.88		
$B_0^{'}$	4.19	4.18		

[a] From the FLAPW–GGA method [37]
[b] From the FLAPW method [37]
[c] From the GGA method [1]
[d] From the LDA method [1]
[e] From the LDA/PW91/PBE/RPBE method [11]
[f] Ref. [38]
[g] Ref. [14]
[h] From the LAPW method [39]
[i] From the LMTO-ASA method [40]
[j] Ref. [41]
[k] Ref. [42]
[m] Ref. [12]

as a function of the pressure. It is found that the transition pressure from the NaCl structure to CsCl structure is about 364.1 GPa. Using the same method, we can obtain the transition pressure of 322.2 GPa for LDA. For comparison, the previous phase transition pressures P_t are also listed in Table 1.

In Fig. 3, for the transition pressure of 364.1 GPa, we illustrate the normalized primitive cell volume V/V_0 (V_0 is the zero-pressure equilibrium primitive cell volume) dependences on pressure P at $T = 300$ and 2,500 K. For comparison, our experimental data observed by RXRD method at $\Psi = 54.7°$ up to 45.4 GPa are also presented. Obviously, as the pressure P increases, the relative volume V/V_0 decreases at a given temperature for the two structures. On the other hand, the partial enlarged view at $T = 300$ K, as an up-right inset to Fig. 3, proves that there exists a volume collapse in volume at phase transition pressure.

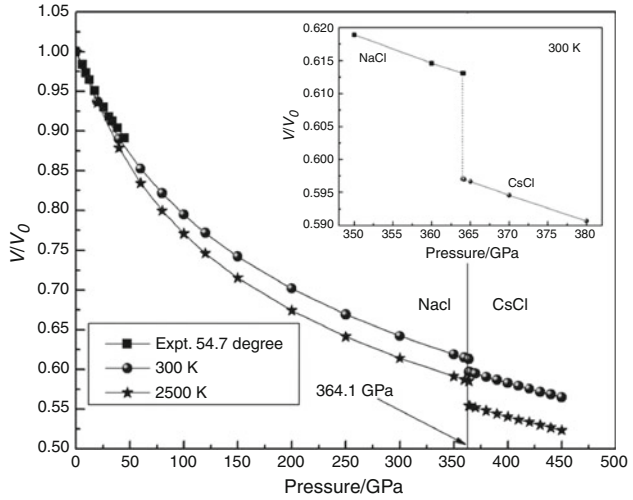

Fig. 3 The normalized primitive cell volume V/V_0 as a function of pressure P for the NaCl and CsCl structures of TiN at $T = 30$; 2,500 K; together with the experimental data up to 45.4 GPa

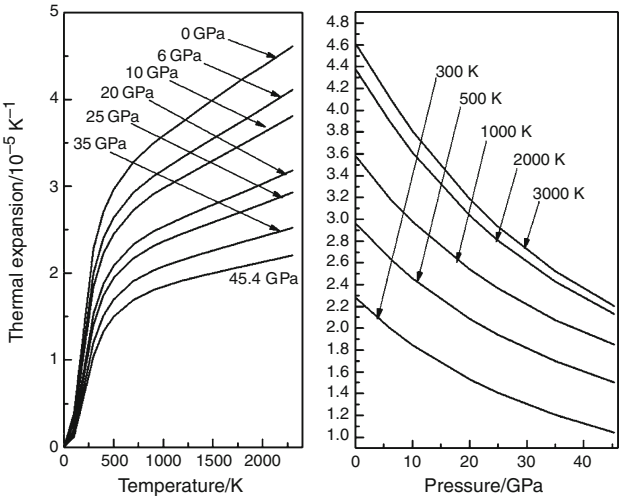

Fig. 4 The thermal expansion (GGA) versus temperature and pressure for TiN

Table 2 The heat capacity C_V/J mol^{-1} K^{-1} and the Debye temperature Θ_D/K over a wide range of temperatures and pressures for the NaCl and CsCl structures of TiN

T/K		P/GPa	0	60	100	300	400	420	450
300	NaCl	C_V	34.51	26.79	23.44	14.28			
		Θ_D	847.76	1133.11	1268.10	1732.32			
	CsCl	C_V					12.44	12.02	11.44
		Θ_D					1857.44	1888.40	1932.80
700	NaCl	C_V	46.55	44.00	42.65	37.46			
		Θ_D	830.15	1124.01	1260.68	1728.50			
	CsCl	C_V					35.98	35.61	35.08
		Θ_D					1854.16	1885.20	1929.83
1,400	NaCl	C_V	49.08	48.37	47.97	46.32			
		Θ_D	798.68	1102.21	1244.16	1718.15			
	CsCl	C_V					45.81	45.68	45.49
		Θ_D					1844.85	1876.06	921.17
2,000	NaCl	C_V	49.51	49.16	48.96	48.11			
		Θ_D	775.69	1082.33	1228.12	1708.43			
	CsCl	C_V					47.85	47.78	47.68
		Θ_D					1835.92	1867.34	1912.80
2,700	NaCl	C_V	49.69	49.51	49.39	48.92			
		Θ_D	756.45	1057.94	1209.11	1696.65			
	CsCl	C_V					48.76	48.73	48.67
		Θ_D					1825.88	1856.85	1903.19

From the quasi-harmonic Debye model, we can determine the thermal expansion coefficient α of TiN at simultaneous extreme pressure P and temperature T conditions, GGA results are shown in Fig. 4. It is noted that at zero pressure α increases exponentially with T at low temperatures and gradually approaches to a linear increase at high temperatures. As the pressure increases, the increase of α with temperature becomes smaller, especially at high temperature. At a given temperature, α decreases strongly with increasing pressure, the thermal expansion coefficient α at 3,000 K is just a little larger than that at 2,000 K, as means that the temperature dependence of α is very small at high temperature and higher pressure.

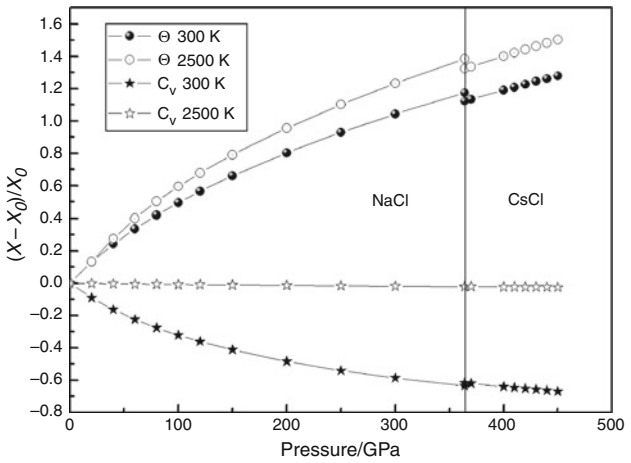

Fig. 5 Variation of thermodynamic parameters X (X: Debye temperature or heat capacity) with pressure P. They are normalized by $(X - X_0)/X_0$, where X and X_0 are the Debye temperature or heat capacity at any pressure P and zero pressure at the temperatures of 300 and 2,500 K

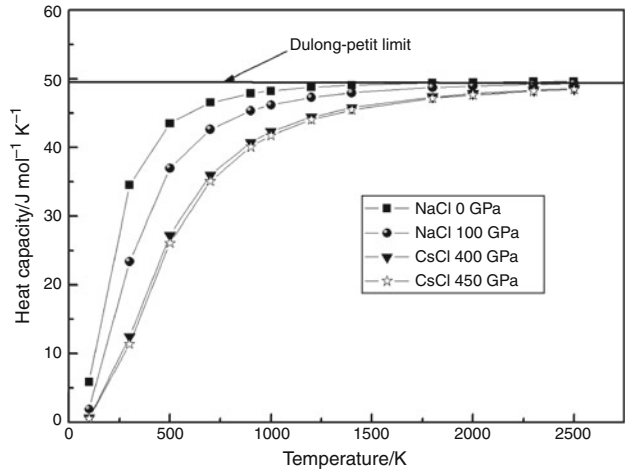

Fig. 6 The heat capacity (GGA) of TiN at various pressures and temperatures

On the other hand, in Table 2, we list the GGA heat capacities and the Debye temperatures at various temperatures (300; 700; 1,400; 2,000; 2,700 K) and pressures (0, 60, 100, 300, 400, 420 and 450 GPa). It is found from Table 2 that the heat capacity C_V in this study is 34.51 Jmol^{-1}K^{-1} at zero pressure and ambient temperature. As pressure increases, the heat capacity C_V decreases and the Debye temperature Θ_D increases. For the NaCl structure, when the applied pressure increases from 0 to 300 GPa, the heat capacities decrease by 58.6, 19.5, 5.6, 2.8, and 1.6% and the Debye temperatures increase by 104.3, 108.2, 115.1, 120.2, and 124.2% at $T = 300$; 700; 1,400; 2,000; and 2,700 K, respectively. Correspondingly, for the CsCl structure, when the pressure from 400 to 450 GPa, the heat capacity decreases by 7.9, 2.5, 0.7, 0.4, and 0.2%, and the Debye temperature increases by 4.06, 4.08, 4.14, 4.19, and 4.23%, respectively.

The variations of the heat capacity C_V and the Debye temperature $\Theta_D$with pressure P both in the NaCl and the CsCl structures for GGA results are shown in Fig. 5. They are normalized by $(X - X_0)/X_0$, where X and X_0 are the heat capacity or Debye temperature at any pressure P and zero pressure. It is shown that, for the two structures of TiN, when the temperature keeps constant, the heat capacity C_V decreases with the applied pressures, as is owing to that the effect of increasing pressure on the material is the same as decreasing temperature of the material. On the other hand, the Debye temperature Θ_D increases almost linearly with applied pressures.

The heat capacity of the NaCl structure and the CsCl structure of TiN for several pressures are plotted in Fig. 6, which shows that when $T < 1{,}800$ K, the heat capacity C_V is dependent on the temperature and pressure. This is because of the anharmonic approximations of the Debye model used here. However, at higher temperatures, the anharmonic effect on C_V is suppressed, as temperature increases, the heat capacity C_V nearly approaches to the Dulong-Petit result 3 k_B ($\approx$49.90 J mol^{-1} K^{-1}), which is followed to all solids at high temperature.

Conclusions

In summary, we have investigated the phase transition of TiN from the NaCl structure to the CsCl structure by the ab initio plane-wave pseudopotential density functional theory method. The pressure of transition from the NaCl structure to the CsCl structure is 364.1 GPa for GGA and 322.2 GPa for LDA from equal enthalpies. Moreover, the dependences of the normalized primitive cell volume on pressure at several temperatures, the Debye temperature $\Theta_D$and heat capacity C_V on the pressure P, and the heat capacity C_V on the temperature T can also be successfully obtained from the quasiharmonic Debye model.

Acknowledegements This study is supported by Scientific Reserch Fund of SiChuan Provincial Education Department (Grant No. 09ZDL01).

References

1. Ahuja R, Eriksson O, Wills JM, Johansson B. Structural, elastic, and high-pressure properties of cubic TiC, TiN, and TiO. Phys Rev B. 1996;53:3072–9.
2. Li X, Kobayashi T, Sekine T. Stability of TiN and fast synthesis of rutile from TiN and CuO by shock compression. Solid State Commun. 2004;130(1–2):79–82.
3. Schwarz K, Crit CRC. Band structure and chemical bonding in transition metal carbides and nitrides. Rev Solid State Mater Sci. 1987;13:211–57.

4. Sempere J, Nomen R, Serra E, Sempere B, Guglielmi D. Thermal behavior of oxidation of TiN and TiC nanoparticles. J Therm Anal Calorim. 2011;105:719–26.
5. Pelletier H, Carradò A, Faerber J, Mihailescu IN. Microstructure and mechanical characteristics of hydroxyapatite coatings on Ti/TiN/Si substrates synthesized by pulsed laser deposition. Appl Phys A. 2011;102:629–40.
6. Hidalgo JA, Montero-Ocampo C, Cuberes MT. Nanoscale visualization of elastic inhomogeneities at TiN coatings using ultrasonic force microscopy. Nanoscale Res Lett. 2009;4:1493–501.
7. Pham VH, Yook SW, Lee EJ, Li Y, Jeon G, Lee JJ, Kim HE, Koh YH. Deposition of TiN films on Co–Cr for improving mechanical properties and biocompatibility using reactive DC sputtering. J Mater Sci Mater Med. 2011. doi:10.1007/s10856-011-4410-8.
8. Price JB, Borland JO, Selbrede S. Properties of chemical-vapor-deposited titanium nitride. Thin Solid Films. 1993;236:311–8.
9. Hegde RI, Fiordalice RW, Travis EO, Tobin PJ. Thin film properties of low-pressure chemical vapor deposition TiN barrier for ultra-large-scale integration applications. J Vac Sci Technol B. 1993;11:1287–96.
10. Oh UC, Je JH. Effects of strain energy on the preferred orientation of TiN thin films. J Appl Phys. 1993;74:1692–6.
11. Marlo M, Milman V. Density–functional study of bulk and surface properties of titanium nitride using different exchange-correlation functionals. Phys Rev B. 2000;62:2899–907.
12. Siegel DJ, Hector LG, Adams JB Jr. Ab initio study of Al–ceramic interfacial adhesion. Phys Rev B. 2003;67:4–092105.
13. Zhao JG, Yang LX, Yu Y, You SJ, Yu RC, Chen LC, Li FY, Jin CQ, Li XD, Li YC, Liu J. Isostructural phase transition of TiN under high pressure. Chin Phys Lett. 2005;22:1199–201.
14. Chauhan R, Singh S, Singh RK. Structural stability of TiO and TiN under high pressure. Cent Eur J Phys. 2008;6:277–82.
15. Vanderbilt D. Soft self-consistent pseudopotentials in a generalized eigenvalue formalism. Phys Rev B. 1990;41:7892–5.
16. Ceperley DM, Alder BJ. Ground state of the electron gas by a stochastic method. Phys Rev Lett. 1980;45:566–9.
17. Perdew JP, Burke K, Ernzerhof M. Generalized gradient approximation made simple. Phys Rev Lett. 1996;77:3865–8.
18. Monkhorst J, Pack JD. Special points for brillouin-zone integrations. Phys Rev B. 1976;13:5188–92.
19. Payne MC, Teter MP, Allen DC, Arias TA, Joannopoulos JD. Iterative minimization techniques for ab initio total-energy calculations: molecular dynamics and conjugate gradients. Rev Modern Phys. 1992;64:1045–97.
20. Milman V, Winkler B, White JA, Packard CJ, Payne MC, Akhmatskaya EV, Nobes RH. Electronic structure, properties, and phase stability of inorganic crystals: A pseudopotential plane–wave study. Int J Quantum Chem. 2000;77:895–910.
21. Lim AR. Thermodynamic properties and phase transitions of Tutton salt $(NH_4)_2Co(SO_4)_2{\cdot}6H_2O$ crystals. J Therm Anal Calorim. 2011. doi:10.1007/s10973-011-1849-2.
22. Atanasova L, Baikusheva-Dimitrova G. Heat capacity and thermodynamic properties of tellurites $Yb_2(TeO_3)_3$, $Dy_2(TeO_3)_3$ and $Er_2(TeO_3)_3$. J Therm Anal Calorim. 2011. doi:10.1007/s10973-011-1325-z.
23. Xue BD, Yang Q, Chen SP, Gao SL. Synthesis, crystal structure, and thermodynamics of a high-nitrogen copper complex with *N*, *N*-bis-(1(2)H-tetrazol-5-yl) amine. J Therm Anal Calorim. 2010;101:997–1002.
24. Knyazev A, Maczka M, Kuznetsova N, Hanuza J, Markin A. Thermodynamic properties of rubidium niobium tungsten oxide. J Therm Anal Calorim. 2009;98:843–8.
25. Blanco MA, Francisco E, Luana V. GIBBS: isothermal–isobaric thermodynamics of solids from energy curves using a quasi-harmonic Debye model. Comp Phys Commun. 2004;158:57–72.
26. Guo HZ, Chen XR, Cai LC, Zhu J, Gao J. Structural and thermodynamic properties of MgB2 from first-principles calculations. Solid State Commun. 2005;134:787–90.
27. Chen XR, Wang HY, Cheng Y, Hao YJ. First-principles calculations for structure and equation of state of MgB_2 at high pressure. Phys B Condens Matter. 2005;307:281–6.
28. Guo HZ, Chen XR, Cai LC, Zhu J, Gao J. First-principles calculations of elastic constants of superconducting MgB_2. Chin Phys Lett. 2005. doi:10.1088/0256-307X/22/7/056.
29. Liu K, He DWN, Zhou XL, Chen HH. First-principles study of structural and thermodynamic properties of osmium. Phys B Condens Matter. 2011;406:3065–9.
30. Hu CE, Zeng ZY, Cheng Y, Chen XR, Cai LC. First-principles calculations for electronic, optical and thermodynamic properties of ZnS. Chin Phys B. 2008. doi:10.1088/1674-1056/17/10/053.
31. Lu LY, Chen XR, Chen Y, Zhou JZ. Transition phase and thermodynamic properties of GaN via first-principles calculations. Solid State Commun. 2005;136:152–6.
32. Blanco MA, Pendás AM, Francisco E, Recio JM, Franco R. Thermodynamical properties of solids from microscopic theory: applications to MgF_2 and Al_2O_3. J Mol Struct (Theochem.). 1996;368:245–55.
33. Flórez M, Recio JM, Francisco E, Blanco MA, Pendás AM. First-principles study of the rock salt–cesium chloride relative phase stability in alkali halides. Phys Rev B. 2002;66:144112/1–8.
34. Francisco E, Sanjurjo M A. Atomistic simulation of SrF2 polymorphs. Phys Rev B. 2001;63:094107/1–9.
35. Chen HH, Peng F, Mao HH, Shen GY, Liermann HP, Li Z, Shu Jf. Strength and elastic moduli of TiN from radial X-ray diffraction under nonhydrostatic compression up to 45 GPa. J Appl Phys. 2010;107:1–5.
36. Birch F. Finite elastic strain of cubic crystals. Phys Rev. 1947;71:809–24.
37. Stampf C, Mannstadt W, Asahi R, Freeman AJ. Electronic structure and physical properties of early transition metal mononitrides: density–functional theory LDA, GGA, and screened-exchange LDA FLAPW calculations. Phys Rev B. 2001;63:155106–11.
38. Gubanov VA, Ivanovsky AL, Zhukov VP. Electronic structure of refractory carbides and nitrides. Cambridge: Cambridge University Press; 1994.
39. Shimizu H, Shirai M, Suzuki N. Electronic, structural and magnetic properties of transition-metal mononitrides. J Phys Soc Jpn. 1997;66:3147–52.
40. Zhukov VP, Gubanov VA, Jepsen O, Christensen NE, Andersen OK. Calculated energy band structures and chemical bonding in titanium and vanadium carbides, nitrides and oxides. J Phys Chem Solids. 1988;49:841–9.
41. Villars P, Calvert LD. Pearson's handbook of crystallographic data for intermetallic phases. 2nd ed. Ohio: ASM International, Materials Park; 1991.
42. Wyckoff RWG. Crystal structures. 2nd ed. New York: Wiley; 1963.